Characterization and Design of Two-Dimensional Electromagnetic Band-Gap Structures by Use of a Full-Wave Method for Diffraction Gratings

Fabrizio Frezza, *Senior Member, IEEE*, Lara Pajewski, and Giuseppe Schettini, *Member, IEEE*

***Abstract*—In this paper, an accurate and efficient characterization of a two-dimensional (2-D) electromagnetic band-gap (EBG) structures is performed, which exploits a full-wave diffraction theory developed for one-dimensional diffraction gratings. EBG materials constituted by 2-D arrays of dielectric rods with arbitrary shape and lattice configuration are analyzed, and the transmission and reflection efficiencies are determined. The high convergence rate of the proposed technique is demonstrated. Results are presented for both TE and TM polarizations, showing the efficiencies as a function of frequency and physical parameters. Comparisons with other theoretical results reported in the literature are shown with a very good agreement, and the authors' theory is also favorably compared with available experimental data. Useful design contour plots are reported by which a very immediate and accurate visualization of the band-gap configurations can be obtained, and design formulas are also included. Finally, the behavioral differences when a periodical defect is present are also highlighted.**

***Index Terms*—Electromagnetic band-gap (EBG) materials, electromagnetic diffraction, gratings, periodic structures.**

I. Introduction

ELECTROMAGNETIC band-gap (EBG) materials [1], also called electromagnetic or photonic crystals or photonic band-gap materials, are periodic structures of great interest for their applications both in the microwave and infrared wavelength ranges. In EBG structures, periodic implants of material with a specific permittivity are embedded in a homogeneous background of different permittivity; the implants are comparable in size to the operation wavelength, and they may be dielectric or metallic, but also magneto-dielectric, ferromagnetic, ferroelectric, or active.

As is known, electromagnetic-wave propagation in EBG materials is analogous to electron-wave propagation in semiconductor crystals: the common feature is the presence of frequency bands within which the waves are highly attenuated and do not propagate [2]. This property is exploited in many electromagnetic and optical applications, such as microwave and millimeter-wave antenna structures [3]–[6], waveguides [7], filters [8], [9], planar reflectors [10], integrated circuits, high- and low-Q resonators [11], quantum optical cavity effects, optical nanocavities, and more. Sonic band-gap materials or artificial acoustic crystal substrates are also being studied [12].

In [13] and [14], reviews of early photonic band-gap research have been collected. In [15]–[17], research on theoretical and numerical methods for the analysis and design of photonic band-gap materials, and also on their applications in the microwave and millimeter frequency range, have been published.

The most commonly used techniques for the analysis and design of EBG materials are the plane-wave-expansion method [1], [18], [19] finite-difference method [20], finite-element method [21], [22], and transfer-matrix method [23], [24]. Various other techniques have been used, such as the effective medium theory [25], phased-array method [26], eigenmode expansion method [6], array scanning method [27], and hybrid methods [28], [29].

It is noted that most EBG applications deal with two-dimensional (2-D) structures, which are invariant along a longitudinal axis and periodic in the transverse plane [20], [30]. A 2-D-EBG structure is easier to manufacture than a three-dimensional one [31], [32]. Moreover, the characterization of structures of finite dimensions is obviously of major practical interest than the determination of absolute band-gaps in infinite structures.

An EBG structure can be considered as a stack of diffraction gratings separated by homogeneous layers, as pointed out in [33], where the rigorous coupled-wave method of Chateau and Hugonin [34], revisited by Peng and Morris [35], and based on a particular S-matrix approach has been employed. The purpose of this paper is to show that accurate, versatile, and fast modeling of finite-thickness (i.e., infinitely extending only in two dimensions) 2-D-EBG structures can be performed by using the full-wave method for one-dimensional diffraction gratings used in [36]. We take advantage of recent calculation techniques to analyze and design, in a stable and rapidly convergent way, electromagnetic crystals with rods that have an arbitrary shape; the rods can form rectangular, triangular, hexagonal, or whatever kind of lattice, and they can be made of isotropic or anisotropic dielectric, as well as metallic material. EBG materials with periodic defects can be studied: EBG structures in which some layers of rods are missing, or are somehow different from the other ones, or else are not perfectly aligned. Defects may be present due to fabrication errors; very often, however, EBG materials with defects are designed on purpose to act as filters or switches since the occurrence of a sharp transmission peak in the band-gap results from defect creation [9], [11].

Manuscript received March 1, 2002; revised October 15, 2002.

F. Frezza and L. Pajewski are with the Department of Electronic Engineering, "La Sapienza" University of Rome, 00184 Rome, Italy (e-mail: fabrizio.frezza@uniroma1.it).

G. Schettini is with the Department of Applied Electronics, "Roma Tre" University of Rome, 00146 Rome, Italy (e-mail: g.schettini@uniroma3.it).

Digital Object Identifier 10.1109/TMTT.2003.808696

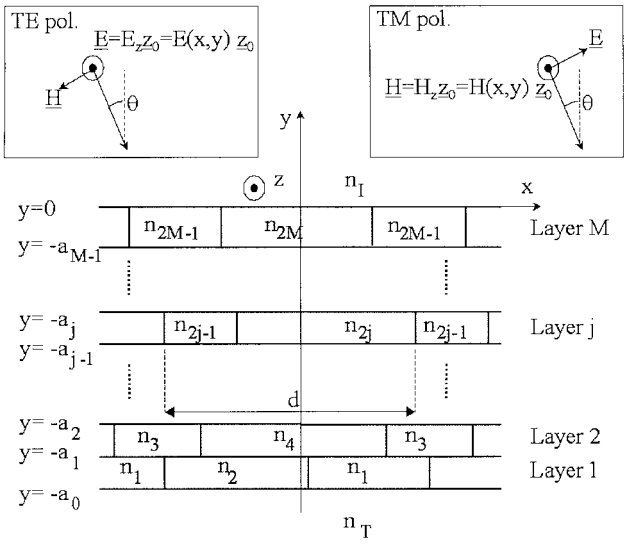

Fig. 1. Geometry of a multilevel grating.

In Section II, we explain how a rigorous diffraction theory for multilevel gratings can be used to model and characterize 2-D-EBG materials. We briefly summarize the formulation of the employed full-wave theory. We also discuss the potentiality of such a method in the analysis and design of EBG structures.

In Section III, we first check the efficiency and accuracy of the approach and numerical implementation that we have developed: convergence figures as well as comparisons with theoretical results and experimental data taken from the literature, are reported and commented on (see Section III-A). A rather complete study of EBG materials made of dielectric parallel rods with a rectangular section is then presented: we investigate the effects of the variation of geometrical and physical parameters, and we give several contour plots as well as design formulas for such structures (see Section III-B). Moreover, we deal with EBG materials with periodic defects and present an example of a structure showing polarization- and frequency-selective properties (see Section III-C).

Finally, in Section IV, concluding remarks are given.

II. Modeling of 2-D-EBG Structures Through a Full-Wave Method for Diffraction Gratings

A 2-D electromagnetic crystal may obviously be considered as a stack of periodic grids of rods separated by homogeneous layers, i.e., as a stack of one-dimensional diffraction gratings. As a consequence, it is clear that 2-D-EBG materials can be analyzed and designed by using a rigorous diffraction theory for multilevel gratings. For a classical reference about the theory of gratings, see [37].

The formulation of the employed method is described in detail in [36]. To summarize, consider a monochromatic plane wave of wavelength λ (in a vacuum), impinging at an angle θ (in the xy-plane) on the multilevel grating of period d shown in Fig. 1. The typical layer j, i.e., the layer located between $y=-a_j$ and $y=-a_{j-1}$ ($1\le j\le M$, where M is the number of layers), is a binary grating including several alternate regions of refractive indexes n_{2j-1} and n_{2j}, respectively. Since the refractive index of the jth layer of the grating, say, $n_j(x)$, is a periodic function, its square and the inverse of its square can be expanded in Fourier series of the form

$$n_j^2(x)=\sum_{m=-\infty}^{+\infty}\alpha_m^{(j)}e^{2\pi imx/d}$$

and

$$n_j^{-2}(x)=\sum_{p=-\infty}^{+\infty}\beta_m^{(j)}e^{2\pi ipx/d} \tag{1}$$

respectively, where $\alpha_m^{(j)}$ and $\beta_m^{(j)}$ are the mth-order Fourier coefficients. The multilevel grating ($-a_0<y<0$) is bounded by two possibly different media having refractive indexes n_I and n_T, respectively.

The problem being 2-D, the incident polarization may be decomposed into the two fundamental TE (electric field parallel to the z-direction) and TM (magnetic field parallel to z) polarizations (see the insets in Fig. 1). The general approach for exactly solving the electromagnetic problem associated with the diffraction grating involves the solution of Maxwell's equations in the incidence region, the M grating layers, and the transmission region.

In the first and last regions, a plane-wave expansion of the electromagnetic fields is employed. For TE polarization, the electric field in the incidence region, say, $E^{(I)}(x,y)$, and in the transmission region, $E^{(T)}(x,y)$, can be written as follows:

$$E^{(I)}(x,y)=e^{i(k_{0x}x-r_0y)}+\sum_{h=-\infty}^{+\infty}R_he^{i(k_{hx}x+r_hy)}, \tag{2}$$

and

$$E^{(T)}(x,y)=\sum_{h=-\infty}^{+\infty}T_he^{i[k_{hx}x-t_h(y+a_0)]} \tag{3}$$

respectively. In (2) and (3), $k_{hx}=(2\pi h/d)+n_Ik\sin\theta$ (Floquet condition) and

$$r_h=\begin{cases}\sqrt{n_I^2k^2-k_{hx}^2}, & n_Ik\ge|k_{hx}|\\ i\sqrt{k_{hx}^2-n_I^2k^2}, & n_Ik<|k_{hx}|\end{cases} \tag{4}$$

$$t_h=\begin{cases}\sqrt{n_T^2k^2-k_{hx}^2}, & n_Tk\ge|k_{hx}|\\ i\sqrt{k_{hx}^2-n_T^2k^2}, & n_Tk<|k_{hx}|\end{cases} \tag{5}$$

with $k=2\pi/\lambda$ and $h=0,\pm1,\pm2,\ldots$. The first term on the right-hand side (RHS) of (2) corresponds to the incident wave, while R_h and T_h are the complex amplitudes of the hth diffraction order in reflection and transmission, respectively.

In the jth layer, we use a modal expansion for the electromagnetic field. For TE polarization, we have

$$E^{(j)}(x,y)=\sum_{m=-\infty}^{+\infty}\sum_{n=-\infty}^{+\infty}E_{mn}^{(j)}e^{ik_{mx}x}\cdot\left[A_n^{(j)}e^{-ik_{ny}^{(j)}(y+a_j)}+B_n^{(j)}e^{ik_{ny}^{(j)}(y+a_{j-1})}\right]. \tag{6}$$

Here, $A_n^{(j)}$ and $B_n^{(j)}$ are the amplitudes of the nth-order eigenmode traveling in the $-y$- and $+y$-direction, respectively; $E_{mn}^{(j)}$ is the mth component of the nth eigenvector, and $k_{ny}^{(j)}$ is the

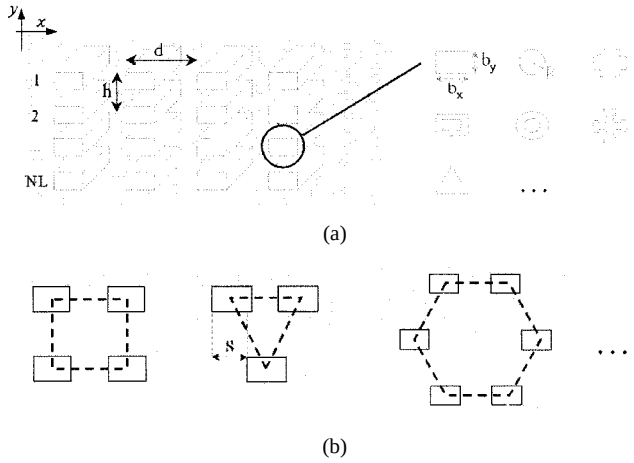

Fig. 2. (a) With the described approach, it is possible to study electromagnetic crystals with rods having an arbitrary shape. (b) The rods can form rectangular, triangular, hexagonal, or whatever kind of lattice.

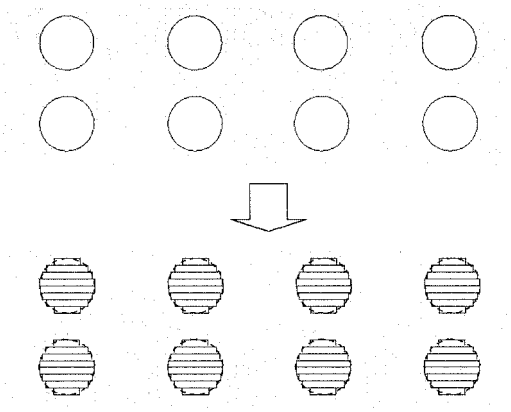

Fig. 3. Discretization of parallel rods having a circular section.

square root (with positive real part) of the nth eigenvalue of the following equation:

$$k_y^{(j)2} E_m^{(j)} + \sum_{p=-\infty}^{+\infty} E_p^{(j)} \left(\delta_{mp} k_{px}^2 - \alpha_{m-p}^{(j)} k^2 \right) = 0 \quad (7)$$

where δ_{mp} is the Kronecker symbol and $m = 0, \pm 1, \pm 2, \ldots$.

The tangential electric- and magnetic-field components have to be matched at all the boundary surfaces. The resulting equation system is to be solved for the reflected and transmitted field amplitudes $\{T_h\}$ and $\{R_h\}$. To overcome numerical problems due to ill-conditioned matrices obtained on imposing the boundary conditions, and to improve numerical stability and efficiency of the implemented codes, we applied the technique presented in [38] to both polarizations.

For TM polarization, the expressions of the magnetic field in the incidence and transmission regions, and in the jth grating layer, are analogous to (2), (3), and (6), respectively.

As is known, the convergence for TM polarization is more critical: to obtain a high convergence rate even in TM polarization, we used the formulation of the eigenvalue problem presented in [39] and [40].

The above-summarized full-wave theory provides a solution of the problem of electromagnetic diffraction by grating structures to an arbitrary degree of accuracy [41].

Our treatment of the EBG structures is very versatile since it allows us to study electromagnetic crystals with rods having an arbitrary shape [see Fig. 2(a)]. Moreover, the rods can form whatever kind of lattice, as sketched in Fig. 2(b). Of course, EBG materials made of holes in a host medium, instead of rods, may also be studied.

In case of EBG structures made of parallel rods with a rectangular section, forming a rectangular or triangular lattice, the application of our method is straightforward and especially fast since only one eigenvalue problem has to be solved.

In case of rods having any shape, the rod section has to be discretized, as shown, e.g., in Fig. 3 for an EBG structure made of parallel rods with a circular section forming a rectangular lattice. It is well known that one can approximate a continuous profile of a diffraction grating by dividing it into a large number of thin planar binary gratings [33]: if each layer is thin enough, the original structure can be analyzed to a high degree of accuracy. Thanks to the stability and robustness of the employed method, in such a discretization, no numerical instability occurs.

As pointed out in Section I, with our approach, EBG materials with periodic defects can be studied. For example, structures in which some layers of rods (as well as layers of the homogeneous background) are missing may be characterized. Moreover, the presence of rods with a shape somehow different from the other ones, as well as the occurrence of layers not perfectly aligned, may be taken into account.

III. Numerical Results

In order to check the efficiency and accuracy of our approach and numerical implementation, here we compare our numerical results with others in the literature, and we also report and comment on some convergence data (see Section III-A). We then study EBG materials made of dielectric parallel rods with a rectangular section (see Section III-B), investigating the effects of the variation of geometrical and physical parameters, and giving efficiency contour plots and design formulas. Moreover, we consider EBG materials that have one periodic defect, showing their polarization- and frequency-selective properties (see Section III-C).

We now introduce some symbols that are used throughout this section (see Fig. 2): b_x and b_y are the dimensions, along x and y, respectively, of a rectangular-section rod; d and h are the periods, along x and y, respectively, of the electromagnetic crystal; R is the radius of a circular-section rod. In a triangular lattice, we assume that there is a lateral shift s between two neighboring layers of rods so that s can vary from zero (when the triangular lattice degenerates in a rectangular one) to $0.5d$. For each geometrical configuration, it is customary to define the so-called filling factor F, which represents the fraction of the unit cell of the periodic structure filled by the rod. The parameter NL represents the number of rod layers in the finite EBG structure. For what concerns the involved materials, n_r and n_b are the refractive indexes of rod and background media, respectively. The discretization parameter D is the number of binary gratings used to approximate a circular-section rod. Moreover, $2N+1$ is the number of diffraction orders taken into account in the calculation. We denote with η_T the total

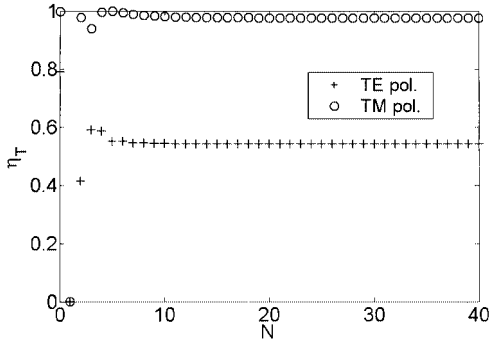

Fig. 4. Convergence of the transmission efficiency η_T as a function of N for an EBG structure made of a stack of $\mathrm{NL} = 10$ layers made of rods with a square section: $d = h = 0.7\lambda, b_x = b_y = 0.5d, n_r = 3.5$, and $n_b = 1$.

transmission efficiency of the EBG structure, which is the sum of the efficiencies of all the transmitted orders (the efficiency of the nth transmitted order is the ratio between the Poynting-vector y-component of the nth-order transmitted wave and that of the incident wave). Analogously, we denote with η_R the total reflection efficiency. From a practical point-of-view, we state the presence of a band-gap when $\eta_T < 0.001$. Unless otherwise specified, the incident plane wave is supposed to impinge normally on the structure $(\theta = 0)$.

A. Convergence, Stability, and Accuracy of Our Approach

An example of convergence of the results, as a function of N, is shown in Fig. 4 for an EBG structure made of a stack of $\mathrm{NL} = 10$ layers (i.e., $M = 19$), made of rods with a square section $d = h = 0.7\lambda, b_x = b_y = 0.5d$. The rod refractive index is $n_r = 3.5$ and the host medium is supposed to be a vacuum $(n_b = 1)$. From Fig. 4, it is seen that the convergence is fast, although the rod refractive index is high. Moreover, it can be appreciated that, using the formulation presented in [39] and [40], we obtain for TM polarization (circles) a rate of convergence similar to the TE-polarization one (crosses). With $N = 24$ and $N = 18$, convergence to the third decimal figure is obtained in TE and TM polarization, respectively. With $N = 32, \eta_T$ assumes a value that is exact within the fourth decimal figure in both polarization cases.

We made a comparison with the results obtained by Peng and Hwang in [42] for an EBG structure of dielectric square-section rods forming a square lattice. In this case, the geometrical and physical parameters are $d = h, b_x = b_y = 0.5d, n_r = 2$, and $n_b = 1$. In Fig. 5(b), η_T is shown as a function of d/λ for TE polarization when $\mathrm{NL} = 10$ (dotted line), $\mathrm{NL} = 20$ (solid line), and $\mathrm{NL} = 30$ (dashed line); the curves can be directly compared with the results of [42, Fig. 3], reported in Fig. 5(a). It can be seen that there is a very good agreement.

Let us consider the structure analyzed in Fig. 5, but with $\mathrm{NL} = 100$. In Fig. 6, we reported η_T as a function of d/λ. Even with such a high number of stacked layers, no numerical instability occurs, showing the robustness of the approach and of the numerical implementation. The possibility to characterize a structure with a very high number of layers is interesting. In fact, the stopbands of such a structure closely approach those of the corresponding infinite EBG material.

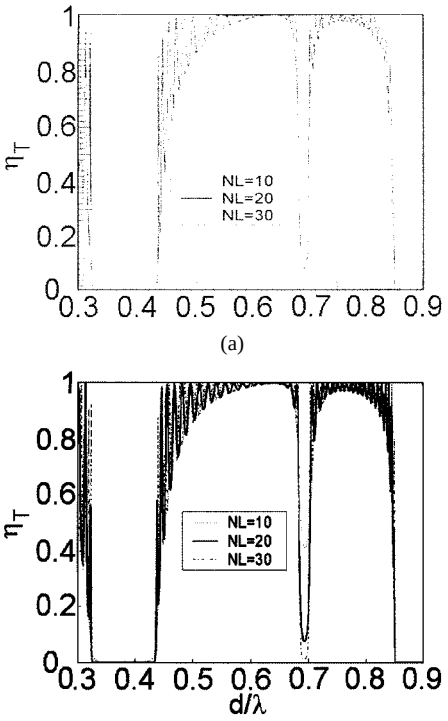

Fig. 5. Comparison between the results obtained by: (a) Peng and Hwang [42] and (b) our results for an EBG structure of dielectric square-section rods forming a square lattice: $d = h, b_x = b_y = 0.5d, n_r = 2$, and $n_b = 1$. The transmission efficiency η_T is shown as a function of d/λ for TE polarization when $\mathrm{NL} = 10$ (dotted line), $\mathrm{NL} = 20$ (solid line), and $\mathrm{NL} = 30$ (dashed line).

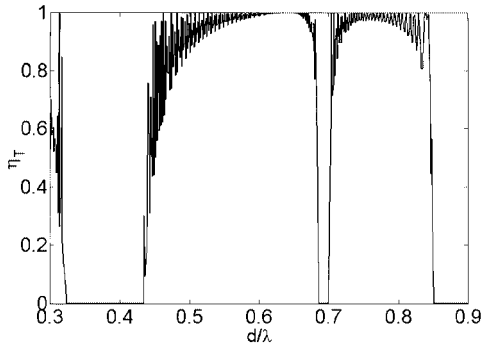

Fig. 6. Same as in Fig. 5, when $\mathrm{NL} = 100$.

To check our codes in the case of cylindrical rods, we made a comparison with the results obtained by Kushta and Yasumoto in [43] for a dielectric-cylinder array immersed in a vacuum; the cylinder radius is $R = 0.3d$ and the cylinder refractive index is $n_r = \sqrt{2}$. In Fig. 7, the reflection efficiency η_R of the array is shown as a function of d/λ for TE polarization; the curve can be directly compared with the results of [43, Fig. 8] (reported in the inset). It can be appreciated that, also in this case, the agreement is very good. We also show in Fig. 8, for the same array of cylinders, with $d = 0.9\lambda$, the convergence of η_R as a function of N for different values of the discretization parameter D.

Finally, we checked our codes in the case of a photonic band-gap structure made of a stack of cylindrical rods forming

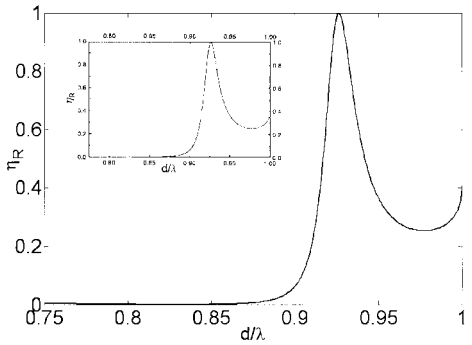

Fig. 7. Comparison with the results obtained by Kushta and Yasumoto [43] (see the inset) for a one-dielectric-cylinder array: $R = 0.3d, n_r = \sqrt{2}$, and $n_b = 1$, TE polarization. The reflection efficiency η_R of the array is shown as a function of d/λ.

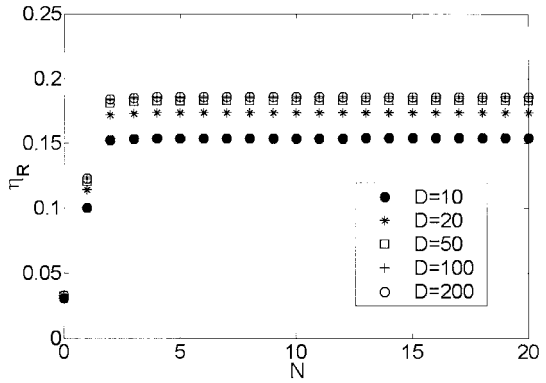

Fig. 8. Convergence of η_R as a function of N for the same array of Fig. 7 when $d = 0.9\lambda$. Different values of the discretization parameter D are considered: $D = 10$ (dots), $D = 20$ (stars), $D = 50$ (squares), $D = 100$ (crosses), and $D = 200$ (circles).

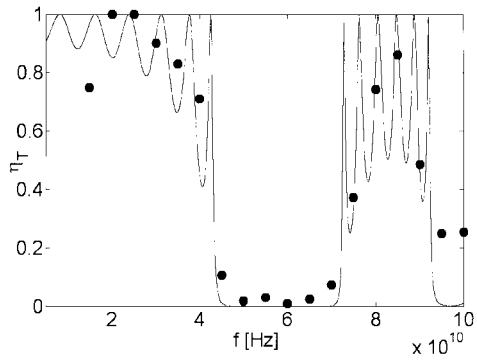

Fig. 9. Comparison with the experimental results obtained by Robertson *et al.* [44] (dots) for TE polarization for a stack of dielectric-cylinder arrays with $d = h = 1.87$ mm, $R = 0.37$ mm, $n_r = 2.98, n_b = 1$, and $\mathrm{NL} = 7$; η_T is shown versus the frequency f.

a square lattice, performing a comparison with the experimental data obtained by Robertson *et al.* in [44] using the coherent microwave transient spectroscopy technique. The geometrical and physical parameters are $d = h = 1.87$ mm, $R = 0.37$ mm, $n_r = 2.98, n_b = 1$, and $\mathrm{NL} = 7$; the polarization is TE. The measurement results were obviously obtained for a finite array of finite-length cylinders: in particular, the sample was 25-columns wide transverse to the direction of propagation, and the rods were 100-mm long. Moreover, the diameter of the rods was $2R \pm 0.03$ mm. In Fig. 9, the transmission efficiency

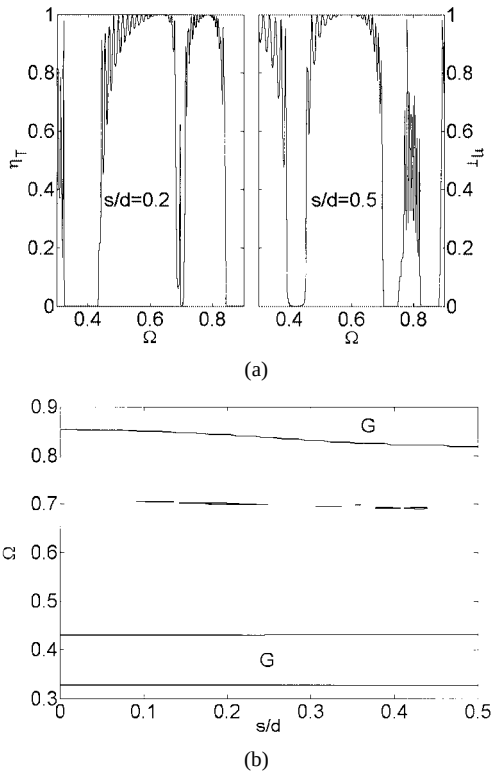

Fig. 10. (a) Transmission efficiency η_T as a function of $\Omega = (\omega d)/(2\pi c)$, c being the light velocity in a vacuum for different values of the normalized shift s/d. The polarization is TE and $\mathrm{NL} = 20$; the other geometrical and physical parameters are the same as in Fig. 5. (b) Contour plot for $\eta_T = 0.001$ as a function of Ω and s/d for the same structure and polarization as in (a). The band-gaps are localized by means of the letter G. The central line in the plot is a very little area in which $\eta_T = 0.001$.

η_T is shown as a function of the frequency f (in hertz); the solid line represents our theoretical calculations, while the dots indicate the measurement results. For what concerns the two dots nearest to $f = 100$ GHz, it can be noticed that our results predict the presence of a quite pronounced stopband, which is not seen experimentally (the dots are well above $\eta_T = 0$). In [44], the authors explained that it was not possible to observe this stopband due to a limitation of their experimental setup. It can be affirmed that our theoretical calculations are in good agreement with the experimental data, showing that our approach can be applied to practical cases.

B. Structures Made of Dielectric Parallel Rods With a Rectangular Section

Starting from the EBG structure considered in Fig. 5, we investigate the effects of the variation of the geometrical and physical parameters. We also give several design contour plots and formulas for such structures.

First of all, we consider the variation of the shift s. In Fig. 10(a), the transmission efficiency η_T is shown as a function of the normalized frequency $\Omega = (\omega d)/(2\pi c) = d/\lambda, c$ being the light velocity in a vacuum for different values of s/d; the polarization is TE and $\mathrm{NL} = 20$. In Fig. 10(b), a contour plot for $\eta_T = 0.001$ as a function of Ω and s/d is shown for the same structure and polarization as in Fig. 10(a); the band-gaps are localized by means of the letter G. In Fig. 11, the same as in Fig. 10(b) is reported for TM polarization.

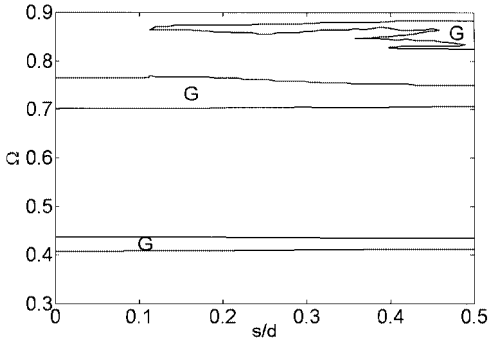

Fig. 11. Same as in Fig. 10(b) for TM polarization.

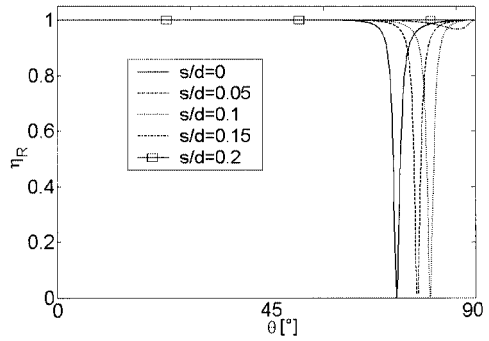

Fig. 12. Reflection efficiency η_R versus the incidence angle θ for the same structure as in Fig. 10, when $\Omega = 0.378$; $s = 0$ (solid line), $s = 0.05d$ (dashed line), $s = 0.1d$ (dotted line), $s = 0.15d$ (dashed–dotted line), and $s = 0.2d$ (solid line with squares).

It can be noted that the parameter s does not have a great effect on the normalized-frequency band-gaps of the structure, especially when the details of the structure are small with respect to the incident wavelength (d/λ small). Due to an averaging phenomenon, the behavior of the EBG structure, for given polarization and incidence angle, depends only on the filling factor and on the refractive index of the rod material, while the rod shape and position become less and less important. The TE gap centered on $\Omega_c = 0.378$ is not affected either in location or in amplitude by the variation of s/d; this stopband is of particular interest due to its width $\Delta\Omega = 0.0964$, which is 25.5% of the central frequency Ω_c. The TM band-gap centered on $\Omega_c = 0.422$ is also almost not affected by the variation of s; this stopband is $\Delta\Omega = 0.0332$ wide, i.e., 7.86% of Ω_c. For what concerns the TE gap, which can be seen at the top of the contour plot in Fig. 10(b), it is noted that a widening of this stopband takes place as s/d increases; at the same time, a TM gap appears [see Fig. 11]. When s/d reaches the maximum value 0.5, this gap is centered on $\Omega_c = 0.853$ and it is $\Delta\Omega = 0.0573$ wide, i.e., 6.71% of Ω_c.

The shift s has an interesting effect on the angular bandwidth of the EBG material. 2-D structures with patterns characterized by different values of s show different performances as the incidence angle varies. To clarify this point, we show in Fig. 12 the reflection efficiency η_R versus the incidence angle θ for the same structure of Fig. 10 when $\Omega = 0.378$ [i.e., we are in the center of the band-gap visible at the bottom of the contour plot of Fig. 10(b)]. We consider several values of the shift s: $s = 0, 0.05d, 0.1d, 0.15d$, and $0.2d$. It is seen that there is an incidence angle around which the structures with $s = 0, 0.05d$, and $0.1d$ yield a transmission peak; this angle is closer to $\theta = 90^o$ as s/d increases, until it disappears. The structure having a pattern characterized by $s = 0.2d$, in fact, exhibits total reflection at any incidence angle, and the same happens for patterns with a higher value of s/d. Therefore, since the value of s/d has not an influence on the location and amplitude of the considered stopband, one can conclude that, in order to obtain at every incidence angle total reflection, it is convenient to choose $s > 0.2d$. It can be useful to give an explicit example showing the physical dimensions of the EBG material that we are considering. At $f = 30$ GHz, in order to obtain $\Omega = 0.378$, the period of the structure should be $d = h = 3.78$ mm; therefore, the dimensions of the square-section rod should be $b_x = b_y = 1.89$ mm and the shift s may be chosen as 0.8 mm or more. Such a structure exhibits total reflection, in case of TE polarization, at every incidence angle and from $f = 26.2$ GHz to $f = 33.8$ GHz.

In other cases, it happens that the incidence angles around which structures with various patterns do not yield a total reflection are different, but present for any value of the normalized shift s/d. In these cases, one can design a composite structure, made of some layers of a rectangular lattice and some of a triangular lattice with a suitable value of s/d in order to obtain a 2-D-EBG material that exhibits total reflection at any incidence angle and without affecting the frequency location and amplitude of the band-gap.

As is known, if band-gaps for both TE and TM polarization states are present and they overlap each other, then their intersections are called complete band-gaps [1]. A large complete band-gap for the structure of Fig. 10 is the one centered on $\Omega_c = 0.416$. This stopband is $\Delta\Omega = 0.0211$ wide, i.e., 5.02% of Ω_c. Moreover, this band-gap is not affected from the variation of s/d, as was just commented on. Another large complete band-gap is present when the shift s/d approaches 0.5. It is centered on $\Omega_c = 0.853$ with $\Delta\Omega = 0.0573$, i.e., 6.72% of Ω_c. Once again, it can be explanatory to give an explicit example showing the physical dimensions of the EBG structure that we are considering. At $f = 30$ GHz, in order to obtain $\Omega = 0.416$, the period of the structure should be $d = h = 4.16$ mm; therefore, the dimensions of the square-section rod should be $b_x = b_y = 2.08$ mm and the shift s may be chosen as 0.83 mm or more. Such a structure exhibits complete total reflection at every incidence angle and from $f = 29.2$ GHz to $f = 30.8$ GHz.

Now, we consider once more the EBG structure of Fig. 5 and study the effects of the variation of the filling factor. In Fig. 13(a), the transmitted efficiency η_T is shown as a function of Ω for different values of $b_x/d = b_y/d$; the polarization is TE and $\mathrm{NL} = 20$. In Fig. 13(b), a contour plot for $\eta_T = 0.001$ as a function of Ω and b_x/d is shown for the same structure and polarization as in Fig. 13(a). Also in this case, the letter G localizes the band-gaps. Moreover, the wider gaps are labeled with a number. In Fig. 14, the same as in Fig. 13(b) is reported for TM polarization.

It can be noted that, for small values of b_x/d, there is no TM gap. As the filling factor increases, there are up to three TM gaps. There are more and wider TE than TM stopbands for small values of the b_x/d. When the filling factor increases, however, there are less differences between the two polarization cases.

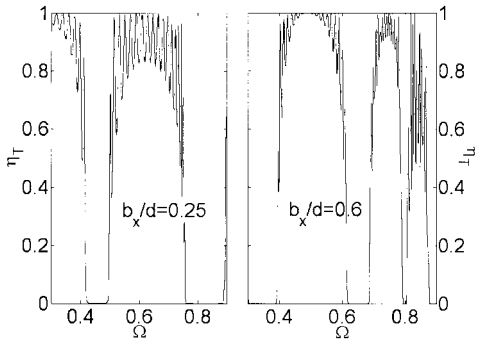

(a)

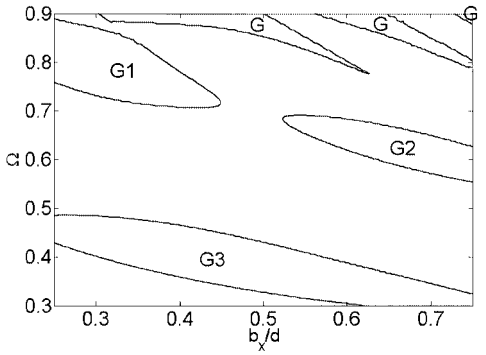

(b)

Fig. 13. (a) Transmission efficiency η_T versus Ω for different values of $b_x/d = b_y/d$. The polarization is TE and $\mathrm{NL} = 20$. The other geometrical and physical parameters are the same as in Fig. 5. (b) Contour plot for $\eta_T = 0.001$ as a function of Ω and b_x/d for the same structure and polarization as in (a). The band-gaps are localized by means of the letter G; the wider gaps are also labeled with a number.

Contour plots like those presented in this paper may be used as design tools. One can deduce from these plots how to build the EBG material in order to satisfy specific requirements. However, it could be very useful to have at one's disposal design formulas, i.e., simple expressions giving location and frequency width of a band-gap as functions of design parameters. To this aim, we made a polynomial curve fitting of our numerical results. The coefficients of the polynomials are chosen fitting the data in a least-square sense. The degree of the polynomials is two. It has been chosen making a compromise between accuracy goals and the will of maintaining simple design formulas. For what concerns the variation of the filling factor, we present formulas for the central frequency Ω_{ci} and the band-gap width $\Delta\Omega_i$, respectively, as functions of b_x/d. The subscript i denotes different gaps with reference to the labels of Figs. 13 and 14 ($i = 1, 2, 3$: TE polarization; $i = 4, 5, 6$: TM polarization); for each formula, the validity range ($\eta_T \leq 0.0001$) is specified. The general expressions are as follows:

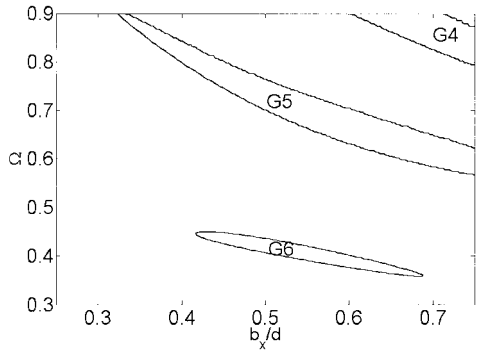

Fig. 14. Same as in Fig. 13(b) for TM polarization.

$$\begin{cases} \Omega_{ci} = A_{2i}\left(\dfrac{b_x}{d}\right)^2 + A_{1i}\dfrac{b_x}{d} + A_{0i} \\ \Delta\Omega_i = B_{2i}\left(\dfrac{b_x}{d}\right)^2 + B_{1i}\dfrac{b_x}{d} + B_{0i} \end{cases} \quad C_{i,\min} \leq \frac{b_x}{d} \leq C_{i,\mathrm{MAX}} \tag{8}$$

The various coefficients of (8) are reported in Table I. The intersection of gaps 2 with 5 gives the location and width of a complete stopband, characterized by (9), shown at the bottom of this page. Moreover, the intersection of gaps 3 with 6 gives the location and width of another complete stopband, with (10), shown at the bottom of this page. Once again, we begin from the EBG structure of Fig. 5 and study the variation of the rod refractive index. In Fig. 15(a), the transmitted efficiency η_T is shown as a function of Ω for different values of n_r. The polarization is TE and $\mathrm{NL} = 20$. In Fig. 15(b), a contour plot for $\eta_T = 0.001$ as a function of Ω and n_r is shown for the same structure and

$$\begin{cases} \Omega_c = -0.2006\left(\dfrac{b_x}{d}\right)^2 - 0.1468\dfrac{b_x}{d} + 0.819 \\ \Delta\Omega = -2.3931\left(\dfrac{b_x}{d}\right)^2 + 3.2525\dfrac{b_x}{d} - 1.0363 \end{cases} \quad 0.524 \leq \frac{b_x}{d} \leq 0.75 \tag{9}$$

$$\begin{cases} \Omega_c = -0.1467\left(\dfrac{b_x}{d}\right)^2 - 0.2059\dfrac{b_x}{d} + 0.5601 \\ \Delta\Omega = -1.3063\left(\dfrac{b_x}{d}\right)^2 + 1.3168\dfrac{b_x}{d} - 0.3078 \end{cases} \quad 0.418 \leq \frac{b_x}{d} \leq 0.617 \tag{10}$$

TABLE I
COEFFICIENTS OF (8)

i	A_{0i}	A_{1i}	A_{2i}	B_{0i}	B_{1i}	B_{2i}	$C_{i,\min}$	$C_{i,\mathrm{MAX}}$
1	0.8781	-0.0276	-0.7455	-0.3311	3.2159	-5.4764	0.25	0.448
2	0.9050	-0.4286	0.0153	-1.0847	3.4056	-2.4862	0.524	0.75
3	0.5329	-0.2797	-0.0491	-0.1347	1.0796	-1.1948	0.25	0.617
4	3.3596	-6.1510	3.7119	-4.0439	11.3458	-7.7959	0.72	0.75
5	1.3527	-1.6935	0.9215	-0.1861	0.8657	-0.7187	0.34	0.75
6	0.5469	-0.1859	-0.1237	-0.3196	1.2970	-1.1994	0.418	0.687

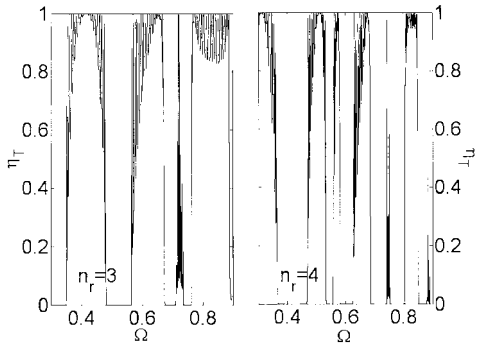

(a)

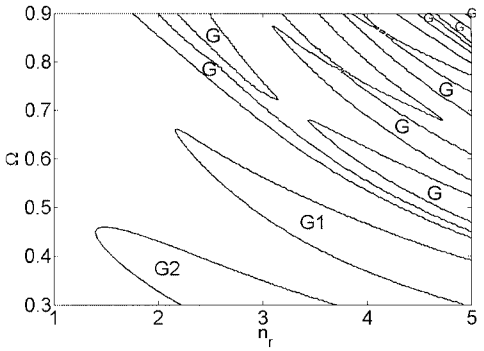

(b)

Fig. 15. (a) Transmission efficiency η_T versus Ω for different values of n_r. The polarization is TE and $\mathrm{NL} = 20$. The other geometrical and physical parameters are the same as in Fig. 5. (b) Contour plot for $\eta_T = 0.001$ as a function of Ω and n_r for the same structure and polarization as in (a). The band-gaps are localized by means of the letter G. The wider gaps are also labeled with a number.

polarization as in Fig. 15(a). The rod refractive index varies from 1 to 5 so that most of the usually employed dielectric materials are considered. Moreover, as in previous plots, the letter G localizes the band-gaps and the wider gaps are labeled with a number. In Fig. 16, the same as in Fig. 15(b) is reported for TM polarization. As expected, when the rod refractive index increases,

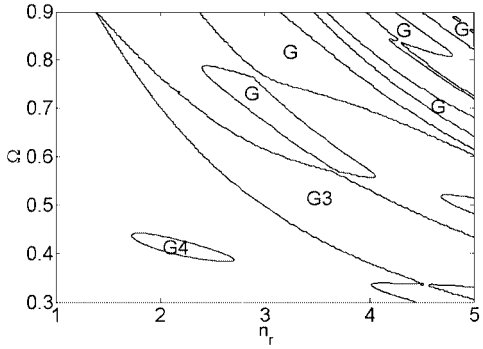

Fig. 16. Same as in Fig. 15(b) for TM polarization.

TABLE II
COEFFICIENTS OF (11)

i	A_{0i}	A_{1i}	A_{2i}	A_{3i}	B_{0i}	B_{1i}	B_{2i}	B_{3i}	$C_{i,\min}$	$C_{i,\mathrm{MAX}}$
1	1.3313	-0.4529	0.0766	-0.0052	-0.5890	0.4806	-0.1110	0.0085	2.17	5
2	0.6589	-0.1720	0.0164	0	-0.5939	0.6486	-0.1493	0	1.4	2.2
3	1.5907	-0.6747	0.1477	-0.0125	-0.0582	0.0252	0.0277	-0.0052	1.42	5
4	0.5535	-0.0764	0.0056	0	-0.3859	0.3835	-0.0879	0	1.74	2.69

the global transmittance of the structure is reduced and the stopbands become more pronounced and numerous in both polarization cases.

Making a polynomial curve fitting of our numerical results plotted in Figs. 15 and 16, we derived some other design formulas of degree 2 or 3 giving location and frequency width of the band-gaps as a function of n_r. The general expressions for Ω_{ci} and $\Delta\Omega_i$ are the following ($i = 1, 2$: TE polarization; $i = 3, 4$: TM polarization), shown in (11), at the bottom of this page. The various coefficients of (11) are reported in Table II. There are no complete band-gaps for results reported in Figs. 15 and 16, up to $n_r \leq 1.74$. There is then a small complete band-gap for $1.74 \leq n_r \leq 2.58$, which is the intersection of gaps 2 and 4, with (12), shown at the bottom of this page. A larger complete band-gap extends in the intersection between gaps 1 and 3. The design formulas giving central frequency and width of this complete stopband are shown in (13), at the top of the following page.

C. EBG Materials With Defects

In this section, we consider an example of an EBG structure that has a periodic defect. As we pointed out in Section I, defects may be present in an electromagnetic crystal due to fabrication errors. Moreover, since the occurrence of sharp transmission peaks in the stopbands results from defect creation, very often

$$\begin{cases} \Omega_{ci} = A_{3i}n_r^3 + A_{2i}n_r^2 + A_{1i}n_r + A_{0i} \\ \Delta\Omega_i = B_{3i}n_r^3 + B_{2i}n_r^2 + B_{1i}n_r + B_{0i} \end{cases} C_{i,\min} \leq \frac{b_x}{d} \leq C_{i,\mathrm{MAX}} \tag{11}$$

$$\begin{cases} \Omega_c = 0.0001n_r^3 - 0.0096n_r^2 + 0.1821n_r - 0.6757 \\ \Delta\Omega = 0.0007n_r^3 - 0.0432n_r^2 + 0.8823n_r - 5.9641 \end{cases} 1.74 \leq n_r \leq 2.2 \tag{12}$$

$$\begin{cases} \Omega_c = -0.0054n_r^3 + 0.0775n_r^2 - 0.45n_r + 1.3283 \\ \Delta\Omega = 0.0090n_r^3 - 0.1128n_r^2 + 0.4747n_r - 0.5830 \end{cases} 2.17 \le n_r \le 5 \tag{13}$$

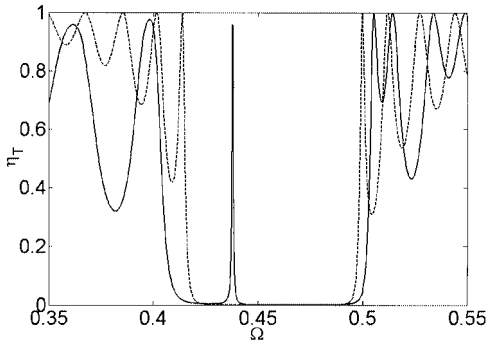

Fig. 17. Transmission efficiency η_T versus d/λ for TE polarization (solid line: structure with a central defect; dashed line: structure without the defect). The geometrical and physical parameters are $\mathrm{NL} = 21$ (so that ten is the number of layers of rods located on each side of a central defect), $n_r = 2, n_b = 1, b_x = b_y = 0.25d, s = 0$, and the refractive index of the defect is $n_d = 2.4$.

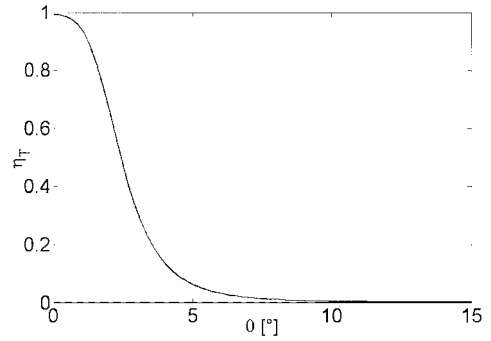

Fig. 18. Transmission efficiency η_T versus the incidence angle θ for the same structure of Fig. 17 when $d/\lambda = 0.438$ (solid line: structure with a central defect; dashed line: structure without the defect). Note that for the structure without the defect, the dashed line is practically coincident with the θ-axis.

EBG materials with defects are designed on purpose to act as filters or switches [9]. With our method, structures in which some layers of rods (as well as layers of the homogeneous background) are missing can be accurately characterized. Moreover, the presence of rods with a shape somehow different from the other ones and the occurrence of layers not perfectly aligned may be taken into account.

We present here the case of an EBG material made of square-section dielectric rods forming a square lattice, in which the defect results from matter excess: in a structure made of an even number of rod layers, the central layer of homogeneous background (i.e., the space between the two central layers of rods) is suppressed. This is equivalent to putting a layer of rods with an anomalous thickness in the middle of the structure. As it will be apparent from the numerical results, such a structure shows polarization- and frequency-selective properties.

The presented structure corresponds to the following parameters: $\mathrm{NL} = 21$ (so that ten is the number of rod layers located on each side of the central defect), $n_r = 2, n_b = 1, b_x = b_y = 0.25d, s = 0$, and the refractive index of the defect is $n_d = 2.4$ (this example is chosen because of the existence, for the structure without defect, of a complete band-gap). The transmission efficiency η_T (solid line) is shown in Fig. 17 as a function of d/λ for TE polarization. One notes, inside the stopband, the presence of a sharp transmission peak (due to the defect) centered on $d/\lambda = 0.438$. The considered structure acts as a filter for TE polarization, while forbidden propagation is kept for TM polarization. In this figure, the behavior of the same structure without the defect is also shown (dashed line) for comparison.

In Fig. 18, η_T is shown as a function of the incidence angle θ, when $d/\lambda = 0.438$, i.e., in correspondence of the transmission peak.

IV. Conclusion

In this paper, a complete characterization of EBG structures constituted by a finite number of periodical layers has been carried out. The analysis employs a very accurate and highly convergent full-wave technique that was developed for the study of diffraction gratings. In particular, we examined here electromagnetic crystals made by a finite number of stacked periodical arrays of dielectric cylinders immersed in a host dielectric medium. The presented results concern rectangular- and circular-section rods, but the technique may be employed for any cross-sectional shape and lattice configuration.

The transmission and reflection efficiencies have been calculated for a variety of cases, and design contour plots and formulas have been reported that are very useful in the design procedure. Comparisons were performed with theoretical results available in the literature, showing very good agreement. A further comparison with some experimental data for a finite-width array of finite-length cylinders is favorable, showing the applicability of the proposed theory to practical devices. An example of a structure with a periodic defect has been considered.

The results of this analysis can be employed in many microwave applications, i.e., filter design, power dividers, planar reflectors, etc. The presented analysis may be applied to other element shapes or lattice configurations, anisotropic dielectrics or metallic materials, and lossy media.

References

[1] J. D. Joannopoulos, R. D. Meade, and J. N. Winn, *Photonic Crystals: Molding the Flow of Light*. Princeton, NJ: Princeton Univ. Press, 1995.

[2] E. Yablonovitch, "Inhibited spontaneous emission in solid-state physics and electronics," *Phys. Rev. Lett.*, vol. 58, pp. 2059–2062, 1987.

[3] W. Y. Leung, R. Biswas, S. D. Cheng, M. M. Sigalas, S. McCalmont, G. Tuttle, and K.-M. Ho, "Slot antennas on photonic band gap crystals," *IEEE Trans. Antennas Propagat.*, vol. 45, pp. 1569–1570, Oct. 1997.

[4] M. Thevènot, C. Cheype, A. Reinex, and B. Jecko, "Directive photonic-bandgap antennas," *IEEE Trans. Microwave Theory Tech.*, vol. 47, pp. 2115–2122, Nov. 1999.

[5] R. Coccioli, F.-R. Yang, K.-P. Ma, and T. Itoh, "Aperture-coupled patch antenna on UC-PBG substrate," *IEEE Trans. Microwave Theory Tech.*, vol. 47, pp. 2123–2130, Nov. 1999.

[6] H.-Y. D. Yang, "Theory of antenna radiation from photonic band-gap materials," *Electromagnetics*, vol. 19, pp. 255–276, May/June 1999.

[7] J. G. Maloney, M. P. Kesler, B. L. Shirley, and G. S. Smith, "A simple description for waveguiding in photonic bandgap materials," *Microwave Opt. Technol. Lett.*, vol. 14, pp. 261–266, Apr. 1997.

[8] S. T. Chew and T. Itoh, "PBG-excited split-mode resonator bandpass filter," *IEEE Microwave Wireless Comp. Lett.*, vol. 11, pp. 364–366, Sept. 2001.
[9] P. Dansas, N. A. Paraire, and S. Laval, "Feasibility of optical filters and switches using plastic photonic bandgap structures," *Proc. SPIE*, vol. 3135, pp. 219–229, 1997.
[10] M. P. Kesler, J. G. Maloney, B. L. Shirley, and G. S. Smith, "Antenna design with the use of photonic band-gap materials as all-dielectric planar reflectors," *Microwave Opt. Technol. Lett.*, vol. 11, pp. 169–174, Mar. 1996.
[11] H. Contopanagos, N. G. Alexopoulos, and E. Yablonovitch, "High Q radio frequency structures using one-dimensionally periodic metallic films," *IEEE Trans. Microwave Theory Tech.*, vol. 46, pp. 1310–1312, Sept. 1998.
[12] C. Rubio, D. Caballero, J. V. Sanchez-Perez, R. Martinez-Sala, J. S. Dehesa, F. Meseguer, and F. Cervera, "The existence of full gaps and deaf bands in two-dimensional sonic crystals," *J. Lightwave Technol.*, vol. 17, pp. 2202–2207, Nov. 1999.
[13] *J. Opt. Soc. Amer. B, Opt. Phys. (Special Issue)*, vol. 10, Feb. 1993.
[14] *J. Mod. Opt. (Special Issue)*, vol. 41, Feb. 1994.
[15] *Electromagnetics (Special Issue)*, vol. 41, Feb. 1999.
[16] *IEEE Trans. Microwave Theory Tech. (Special Issue)*, vol. 47, Nov. 1999.
[17] *J. Lightwave Technol. (Special Section)*, vol. 17, Nov. 1999.
[18] K. M. Ho, C. T. Chan, and C. M. Soukoulis, "Existence of a photonic bandgap in periodic dielectric structures," *Phys. Rev. Lett.*, vol. 65, pp. 3152–3155, 1990.
[19] B. A. Munk and G. A. Burrell, "Plane-wave expansion for arrays of arbitrarily oriented piecewise linear elements and its application in determining the impedence of a single linear antenna in a lossy half-space," *IEEE Trans. Antennas Propagat.*, vol. AP-27, pp. 331–343, May 1979.
[20] H. Y. D. Yang, "Finite difference analysis of 2-D photonic crystals," *IEEE Trans. Microwave Theory Tech.*, vol. 44, pp. 2688–2695, Dec. 1996.
[21] R. Coccioli, T. Itoh, and G. Pelosi, "A finite element-generalized network analysis of finite thickness photonic crystals," in *IEEE MTT-S Int. Microwave Symp. Dig.*, 1997, pp. 195–198.
[22] G. Pelosi, A. Cocchi, and A. Monorchio, "A hybrid FEM-based procedure for the scattering from photonic crystals illuminated by a Gaussian beam," *IEEE Trans. Antennas Propagat.*, vol. 48, pp. 973–980, June 2000.
[23] J. B. Pendry and A. MacKinnon, "Calculation of photon dispersion relations," *Phys. Rev. Lett.*, vol. 69, pp. 2772–2775, 1992.
[24] J. B. Pendry, "Photonic structures," *J. Mod. Opt.*, vol. 41, pp. 209–229, Feb. 1994.
[25] P. Lalanne, "Effective medium theory applied to photonic crystals composed of cubic or square cylinders," *Appl. Opt.*, vol. 35, pp. 5369–5380, Sept. 1996.
[26] C. Caloz, A. K. Skrivervik, and E. Gardiol, "An efficient method to determine Green's functions of a two-dimensional photonic crystal excited by a line source—The phased-array method," *IEEE Trans. Microwave Theory Tech.*, vol. 50, pp. 1380–1391, May 2002.
[27] T. Suzuki and P. K. L. Yu, "Emission power of an electric dipole in the photonic band structure of the FCC latice," *J. Opt. Soc. Amer. B, Opt. Phys.*, vol. 12, pp. 570–582, Apr. 1995.
[28] S. D. Gedney, J. F. Lee, and R. Mittra, "A combined FEM/MoM approach to analyze the plane wave diffraction by arbitrary gratings," *IEEE Trans. Antennas Propagat.*, vol. 40, pp. 363–370, Feb. 1992.
[29] E. W. Lucas and T. P. Fontana, "A 3-D hybrid finite element/boundary element method for the unified radiation and scattering analysis of general infinite periodic arrays," *IEEE Trans. Antennas Propagat.*, vol. 43, pp. 145–153, Feb. 1995.
[30] M. Sarnowski, T. Vaupel, V. Hansen, E. Kreysa, and H. P. Gemuend, "Characterization of diffraction anomalies in 2-D photonic bandgap structures," *IEEE Trans. Microwave Theory Tech.*, vol. 49, pp. 1868–1872, Oct. 2001.
[31] S. Y. Lin, G. Arjavalingam, and W. M. Robertson, "Investigation of absolute photonic band-gaps in 2-dimensional dielectric structures," *J. Mod. Opt.*, vol. 41, pp. 385–393, Feb. 1994.
[32] J. B. Nielsen, T. Søndergaard, S. E. Barkou, A. Bjarklev, J. Broeng, and M. B. Nielsen, "Two-dimensional Kagomé structure, fundamental hexagonal photonic crystal configuration," *Electron. Lett.*, vol. 35, pp. 1736–1737, Sept. 1999.
[33] P. Dansas and N. Paraire, "Fast modeling of photonic bandgap structures by use of a diffraction-grating approach," *J. Opt. Soc. Amer. A, Opt. Image Sci.*, vol. 15, pp. 1586–1598, June 1998.
[34] N. Chateau and J.-P. Hugonin, "Algorithm for the rigorous coupled-wave analysis of grating diffraction," *J. Opt. Soc. Amer. A, Opt. Image Sci.*, vol. 11, pp. 1321–1331, Apr. 1994.
[35] S. Peng and G. M. Morris, "Efficient implementation of rigorous coupled-wave analysis for surface-relief gratings," *J. Opt. Soc. Amer. A, Opt. Image Sci.*, vol. 12, pp. 1087–1089, May 1995.
[36] R. Borghi, F. Frezza, L. Pajewski, M. Santarsiero, and G. Schettini, "Full-wave analysis of the optimum triplicator," *J. Electromagn. Waves Applicat.*, vol. 15, pp. 689–707, May 2001.
[37] R. Petit, "Electromagnetic theory of gratings," in *Topics in Current Physics*, Berlin, Germany: Springer-Verlag, 1980.
[38] M. G. Moharam, D. A. Pommet, E. B. Grann, and T. K. Gaylord, "Stable implementation of the rigorous coupled-wave analysis for surface-relief gratings: Enhanced transmittance matrix approach," *J. Opt. Soc. Amer. A, Opt. Image Sci.*, vol. 12, pp. 1077–1086, May 1995.
[39] P. Lalanne and G. M. Morris, "Highly improved convergence of the coupled-wave method for TM polarization," *J. Opt. Soc. Amer. A, Opt. Image Sci.*, vol. 13, pp. 779–784, Apr. 1996.
[40] G. Granet and B. Guizal, "Efficient implementation of the coupled-wave method for metallic lamellar gratings in TM polarization," *J. Opt. Soc. Amer. A, Opt. Image Sci.*, vol. 13, pp. 1019–1023, 1996.
[41] L. Li, "Justification of matrix truncation in the modal methods of diffraction gratings," *Pure Appl. Opt.*, vol. 1, pp. 531–536, July 1999.
[42] S. T. Peng and R. B. Hwang, "Dispersion characteristics of two-dimensionally periodic structures," in *Proc. URSI Int. Electromagnetic Theory Symp.*, Victoria, BC, Canada, May 2001, pp. 317–319.
[43] T. Kushta and K. Yasumoto, "Electromagnetic scattering from periodic arrays of two circular cylinders per unit cell," *PIER*, vol. 29, pp. 69–85, 2000.
[44] W. M. Robertson, G. Arjavalingam, R. D. Meade, K. D. Brommer, A. M. Rappe, and J. D. Joannopoulos, "Measurement of photonic band structure in a two-dimensional periodic dielectric array," *Phys. Rev. Lett.*, vol. 68, pp. 2023–2027, Mar. 1992.

Fabrizio Frezza (S'87–M'90–SM'95) received the Laurea degree (*cum laude*) in electronic engineering and the Doctorate in applied electromagnetics from "La Sapienza" University of Rome, Rome, Italy, in 1986 and 1991, respectively.

In 1986, he joined the Electronic Engineering Department, "La Sapienza" University of Rome, where he was a Researcher from 1990 to 1998, a temporary Professor of electromagnetics from 1994 to 1998, and an Associate Professor since 1998. His main research activity concerns guiding structures, antennas and resonators for microwaves and millimeter waves, numerical methods, scattering, optical propagation, plasma heating, and anisotropic media.

Dr. Frezza is a member of Sigma Xi, the Electrical and Electronic Italian Association (AEI), the Italian Society of Optics and Photonics (SIOF), the Italian Society for Industrial and Applied Mathematics (SIMAI), and the Italian Society of Aeronautics and Astronautics (AIDAA).

Lara Pajewski received the Laurea degree (*cum laude*) in electronic engineering from the "Roma Tre" University, Rome, Italy, in 2000, and is currently working toward the Ph.D. degree in applied electromagnetics at "La Sapienza" University of Rome, Rome, Italy.

In 2000, she joined the Department of Electronic Engineering, "La Sapienza" University of Rome. Her main research interests are electromagnetic analysis of periodic structures, scattering problems, and numerical methods.

Giuseppe Schettini (S'82–M'96) received the Laurea degree (*cum laude*) in electronic engineering, Ph.D. degree in applied electromagnetics, and Laurea degree (*cum laude*) in physics from "La Sapienza" University of Rome, Rome, Italy, in 1986, 1992, and 1995, respectively.

Upon his graduation in electronic engineering, he joined the Italian Energy and Environment Agency (ENEA), where he was initially involved with free electron generators of millimeter waves and then microwave components and antennas for the heating of thermonuclear plasmas. In 1992, he joined "La Sapienza" University as a Researcher of electromagnetics. From 1995 to 1998, he has been a temporary Professor of electromagnetics. Since 1998, he has been an Associate Professor of antennas and of microwaves at the "Roma Tre" University of Rome, Rome, Italy. His scientific research is focused on scattering from cylindrical structures, ferrite resonators, electromagnetic analysis of diffractive optics, numerical methods, and antennas.

Dr. Schettini is a member of the IEEE Antennas and Propagation Society (IEEE AP-S) and the IEEE Microwave Theory and Techniques Society (IEEE MTT-S).